Accounting for local interactions in the prediction of roping of ferritic stainless steel sheets

Accounting for local interactions in the prediction of roping of ferritic stainless steel sheets

G Lefebvre[1], C W Sinclair[1], R A Lebensohn[2] and J-D Mithieux[3]

[1] Department of Materials Engineering, The University of British Columbia, Vancouver, V6T1Z4, Canada
[2] Materials Science and Technology Division, Los Alamos National Laboratory, MS G755, Los Alamos, NM 87545, USA
[3] Aperam Stainless Steel Research Center, Isbergues, France

E-mail: glefe220@interchange.ubc.ca

Abstract

The effect of the spatial distribution of crystallographic orientations on roping amplitude and wavelength in ferritic stainless steel has been evaluated. The through-thickness mechanical behaviour of a sheet deformed in tension has been tested experimentally and simulated using a full-field viscoplastic fast Fourier transform formulation. These crystal plasticity simulations use orientation imaging microscopy data as input, allowing for large-scale simulation domains to be investigated while accounting for the clustering of orientations with similar deformation behaviour. The simulations predict both the local deformation response as well as the macroscopic surface roughness. The latter is compared quantitatively with experimental measurements and is shown to predict both the wavelength and amplitude of the observed roping. The results of these simulations have also been compared with previously proposed mean-field crystal plasticity simulations of roping, performed using the viscoplastic self-consistent code, in which each crystal orientation is, at most, influenced by the behaviour of a homogenized matrix, but not by its local neighbourhood. Comparison between these two kinds of approaches thus allows us to assess the significance of the local neighbourhood on the macroscopic prediction of roping.

(Some figures may appear in colour only in the online journal)

1. Introduction

The phenomenon known as 'roping' or 'ridging' [1–3] is most commonly observed as raised 'rope-like' or 'ridge-like' features running parallel to the prior rolling direction (RD) on the surface of ferritic stainless steel sheet following stretching operations. The terms 'roping'
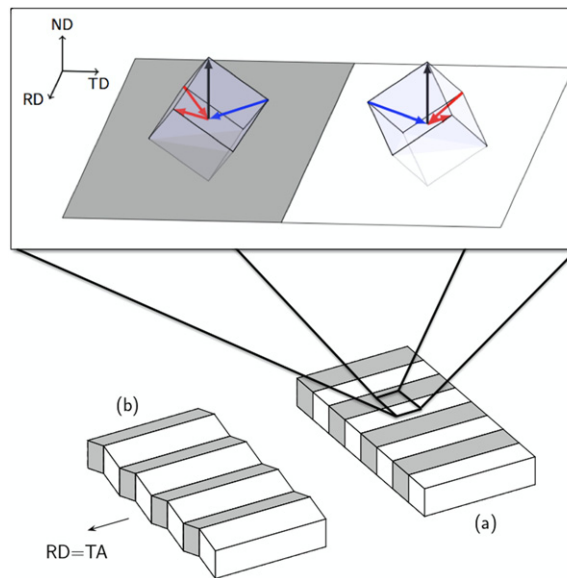
Figure 1. The Takechi model for roping envisions parallel bands of grains along the prior RD which is taken to be parallel to the TA. Alternating grains with different variants of the $\{1\,1\,1\}\langle 1\,1\,0\rangle$ orientation (grey and white) have enantiomorphically oriented slip directions (i.e. they are mirror images). During a tensile test performed parallel to RD the two variants tend to have a net out-of-plane shear in opposite directions resulting in a corrugation of the sheet (*b*). The inset schematically illustrates the orientations of the $\langle 1\,1\,1\rangle$ slip directions in two variants of $\{1\,1\,1\}\langle 1\,1\,0\rangle$ misoriented by $180°$ about ND. In this case the two red slip directions cause elongation parallel to the TA but no contraction parallel to ND or TD. For contraction the blue slip direction has to operate but this results in an unbalanced out-of-plane shear that leads to a rigid rotation in opposite directions for the grey and white grains. The result on a macroscopic scale is the bending or corrugation of the sheet as illustrated in (*b*).

and 'ridging' were used as descriptive terms with reference to the surface appearance after stretching. The wavelength of this anisotropic surface roughness is much larger than the characteristic length-scale of the microstructure, being on the order of 1 mm. The amplitude of the roughness, on the other hand, tends to vary but is generally in the range of ∼5 and 50 μm. While roping appears to the observer as a sort of surface roughness, it is in fact a consequence of an organized through-thickness deformation of the sheet resulting in the raised 'ridges' on one side of the sheet corresponding to 'troughs' on the other side of the sheet. This is to be contrasted with other forms of surface roughening which can show local thinning or uncorrelated surface roughness on the top and bottom surfaces of sheet, e.g. [4].

It is generally accepted that the appearance of roping is associated with clustering of grains having a similar tendency for deformation [1–3, 5, 6]. Of the early proposals forwarded to explain this inhomogeneous deformation, it is the concept originally proposed by Takechi *et al* [1] that most closely resembles what is observed experimentally. In the original Takechi model, the through-thickness corrugation of the material is attributed to bands of grains having crystallographic orientations whose slip systems are enantiomorphically oriented about the RD (figure 1). When tension is imposed parallel to the length of the bands (the bands experimentally found to be parallel to the prior RD), there is a net out-of-plane shearing tendency induced, causing a rigid rotation of the grains about the long axis of the bands.

Given the importance of crystallographic orientation to roping, several attempts have been made to quantitatively link microtexture to roping using crystal plasticity simulations. Engler

et al [7] used the viscoplastic self-consistent (VPSC) code [8, 9] to identify grain clusters having a high tendency for through-thickness shearing from two-dimensional electron backscatter diffraction (EBSD) data, collected from the normal direction (ND) plane (the plane containing the rolling (RD) and transverse (TD) directions) of an AISI 430 ferritic stainless steel sheet. While previous studies had focused on orientation data alone to identify clustering of grains with similar orientations, the work of Engler *et al* [7] was among the first to definitively show large-scale clustering of grains with a strong out-of-plane shearing tendency lying in bands parallel to the RD.

While these results obtained with the VPSC code were mapped back onto the original EBSD data to give an impression of the spatial distribution of the shearing tendency, no explicit spatial correlation between grains and their surroundings was included in these simulations. A fundamental aspect of mean-field calculations, like the ones carried out using VPSC, is that they are performed under conditions where individual crystal orientations are embedded in a homogeneous effective medium whose properties are those of the average polycrystalline material. Thus, the ability to explicitly examine the effect of the local environment on the shearing tendency of individual grains could not be captured, and quantitative predictions of surface roughness amplitude or wavelength could not be made.

Several attempts have been made to incorporate the three-dimensional microstructure and spatial information into the problem of roping using full-field crystal plasticity finite element (CPFEM) calculations. These have generally been limited to highly simplified simulations performed on scales much smaller than the scale of 'real' microstructures due to restrictions on computational resources, e.g. [10]. Notable among the CPFEM calculations are the two-dimensional calculations performed by Wu *et al* [11, 12] on data similar to that used by Engler *et al* [7] in an attempt to explicitly incorporate the spatial correlation between bands. Large EBSD maps measured on the ND plane of an AISI 430 stainless steel sheet were used as the input for the crystal plasticity calculations. The size of the simulation box required to capture the scale of roping precluded a direct three-dimensional calculation of the shearing tendency. Instead, smaller scale simulations were performed on individual orientations to assess the shearing tendency of individual orientations. This pre-computed 'simple ridging model' was then used in place of direct crystal plasticity simulations on the full EBSD map to predict shearing tendency.

In both cases described above the calculation domains were limited to the sheet plane, meaning the potential influence of the microstructure and microtexture through the sheet thickness was not taken into account. It is known empirically, however, that the microstructure through the sheet thickness has a significant effect on the characteristics of roping. In an attempt to specifically look at the importance of local environment on the tendency for individual grains to shear, Sinclair [13] used the VPSC code with idealized microstructures to study the deformation behaviour of individual grains embedded within different media. Grains having a strong shearing tendency were embedded within a matrix having either a strong opposite shearing tendency or no shearing tendency. From these simulations it was shown that the tendency for shearing in orientations such as $\{1\,1\,1\}\langle1\,1\,0\rangle$ was far stronger than the tendency for no shearing in grains having orientations such as $\{1\,1\,1\}\langle1\,1\,2\rangle$, this result being explained by the difference in the slope of Taylor factor with respect to shear component of the deformation gradient [13]. These results indicated that the grains having no net tendency for shearing would shear if placed adjacent to grains having a strong shearing tendency, thereby increasing the number of grains contributing to the net shearing behaviour. It was also shown that the length of the grain clusters parallel to the RD of the sheet, while likely being important for the visual appearance of the surface, did not strongly affect the tendency grain rotation.

The above simulations have greatly advanced our understanding of the phenomenon of roping, yet our ability to perform fully resolved crystal plasticity calculations on real microstructures over length-scales appropriate to replicate the wavelength and amplitude of roping has remained out of reach. To overcome this limitation, in this paper we have studied the problem of roping with a highly efficient full-field model for the prediction of the viscoplastic (VP) deformation of polycrystals based on the fast Fourier transform (FFT) algorithm [14], which can use direct input from a polycrystal's orientation image [15]. These characteristics make the viscoplastic fast Fourier transform (VPFFT) model ideal for examining the phenomenon of roping starting from a large-scale experimentally measured microstructure.

Following on the work of Sinclair [13], this work seeks to examine the role of local environment of individual grains on the tendency for shearing by examining the information contained in the RD plane (plane containing the ND and TD) of the sheet as opposed to the more commonly examined ND plane. EBSD maps measured on this plane are used for input to crystal plasticity simulations. While three-dimensional EBSD datasets are becoming more common [16–18], the capability to acquire and simulate volumes representative of the roping phenomenon remain largely out of reach. The results of these simulations are used to predict the surface displacements corresponding to roping during a tensile test and are compared quantitatively with experimentally measured surface profiles measured from the same material. To assess the influence of the local grain-to-grain interactions, as captured by the VPFFT model, comparisons with VPSC crystal plasticity simulations were also conducted, in which local neighbour interactions are not accounted for.

While this paper focuses on the effect of local shearing as a source of roping, the simulation approaches used capture the full deformation field at each point in the domain. The predicted surface roughening therefore arises as a consequence of the full deformation response at each point through thickness.

2. Experimental characterization of microstructure and roping

A 1.4 mm thick sheet of AISI 409 ferritic stainless steel (containing approximately 12 wt%Cr) was provided by the Aperam Stainless Steel Research Centre (Isbergues France) under the as-cold rolled and annealed condition. The grain size of the material, measured as the equal area diameter from EBSD maps (figure 3(*b*)), was 23 μm. This material was specifically selected as it exhibited roping with exceptionally high amplitude. Three pole figures ($\{1\,1\,0\}$, $\{2\,1\,1\}$ and $\{2\,0\,0\}$) measured by x-ray diffraction on a sample's mid-thickness and at the sheet's surface were used to compute the orientation distribution function (ODF) using the Bruker TexEval software with $L_{max} = 22$. The bulk texture (figure 2) is typical of that observed in recrystallized ferritic stainless steel sheet. A shifted γ-fibre texture having a maximum intensity close to $\{2\,2\,3\}\langle 5\,8\,2 \rangle$ is observed in both the near surface and centre of the sheet.

EBSD was used to characterize the microstructure of this material in its as-received state. Samples were prepared by mechanical polishing followed by electropolishing in a solution of 5% perchloric acid in acetic acid at 15 V. Both the ND surface (the surface containing the RD and TD directions) and the RD surface (the surface containing the ND and TD directions) were prepared for observation. In the case of the ND surface, the material was first mechanically polished to the mid-plane prior to electropolishing. Observations were made using a Hitachi H-570 scanning electron microscope equipped with the HKL Channel 5 software for acquisition and post-processing. The microstructures viewed in the ND and RD planes are shown in figure 3 in the form of inverse pole figure maps where the colour code corresponds to crystallographic directions parallel to the ND of the sheet according to the accompanying colour scheme. In the case of the RD plane map, EBSD measurements were made over approximately three quarters
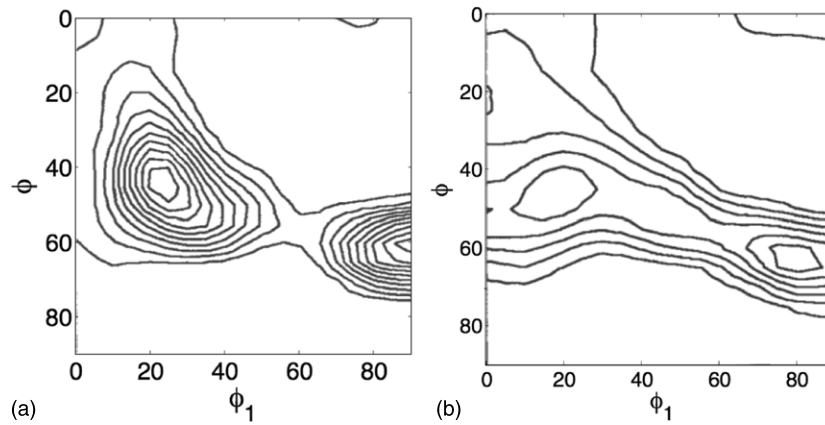
Figure 2. Bulk textures as measured by x-ray diffraction at (*a*) the centre of the as-received sheet and (*b*) the surface of the as-received sheet. Here the $\phi_2 = 45°$ section of the ODF is shown illustrating the shifted γ-fibre texture where the maximum in intensity is located close to the orientation $\{2\,2\,3\}\langle5\,8\,2\rangle$. The contour levels are at $f(g) = 1.15$, 2.32, 3.49, 4.65, 5.82, 6.98, 8.15, 9.31, 10.48 and 11.65.

of the thickness of the sample. Thus, the EBSD map in this case is 1.04 mm thick rather than the full 1.4 mm thickness of the starting sheet.

As is common in ferritic stainless steel sheets, the ND plane EBSD map (figure 3(*a*)) reveals an apparent clustering of grains with near γ-fibre orientations in bands parallel to the prior RD. When viewed in the RD plane, however, no obvious banding or clustering is observed through thickness. In the RD plane a distribution in the grain size is observed, with smaller grains observed closer to the sheet surfaces and coarser grains near the centre of the sheet.

From the material described above, tensile tests were performed at room temperature using large tensile test samples (250 mm gauge length by 50 mm gauge width). Room temperature tensile tests were performed to 15% strain at a strain rate of approximately 10^{-3} s^{-1} with the tensile axis (TA) parallel to the prior RD, at 45° from RD, and parallel to TD. Profilometry measurements were made on one side of the sample using a Taylor-Hobson Talysurf contact profilometer. A form removal using a second order polynomial was first applied to the measured data. Gaussian filtering was subsequently performed to remove high-frequency noise. The two-dimensional surface roughness measured on these samples is illustrated in figure 4. One can see the strong change in the appearance of the surface for the three testing directions. Very strong roping appears on the sample tested parallel to RD. From these data a root mean square amplitude, defined as

$$R_q = \sqrt{\frac{1}{A} \int_0^{x_{\max}} \int_0^{y_{\max}} (Z(x, y) - \bar{Z})^2 \cdot \mathrm{d}x \cdot \mathrm{d}y} \tag{1}$$

was measured and found to be $R_q = 18\,\mu$m. Taking the Fourier transform of the average two-dimensional roughness profile (figure 4(*d*)) allows a characteristic wavelength at 3.86 and 5.4 mm to be identified. As the tensile direction is rotated by 45° one observes a significant drop in the amplitude of the roping, but a continued directionality of the surface roughness parallel to the prior rolling direction. Finally, testing parallel to TD results in a much lower amplitude and more isotropic appearance of the surface roughness.
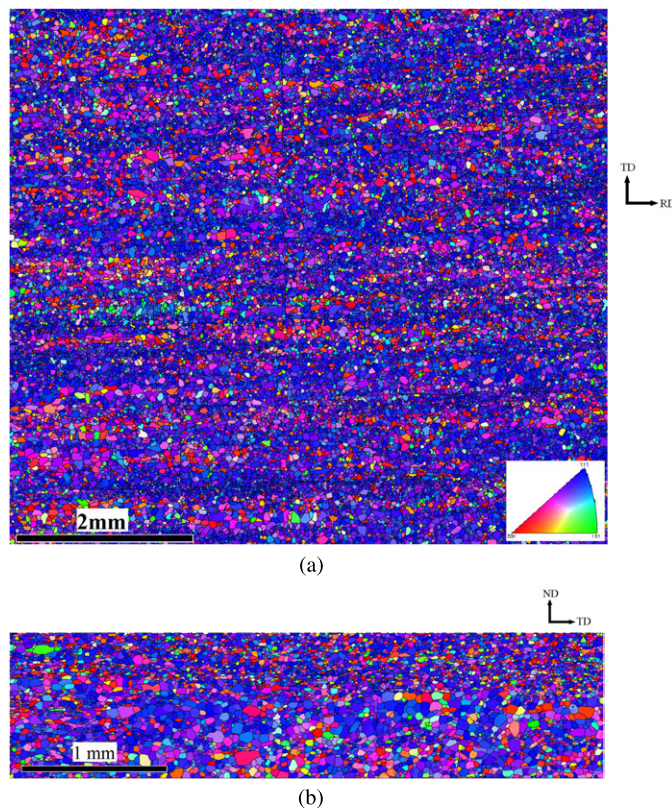
(a)

(b)

Figure 3. EBSD maps measured on the (*a*) ND plane at the mid-plane of the sheet and (*b*) RD plane of the sheet. In the online version, the colouring corresponds to crystallographic directions parallel to the ND, the scheme given by the inset in (*a*). In the print version, the grey regions correspond to grains within 15° of the γ-fibre. The maps indicate a high propensity for grains to be near the γ-fibre, ND||{1 1 1}, consistent with figure 2. While there is an apparent clustering of γ-fibre grains parallel to the RD in the ND plane, no obvious through thickness.

3. Crystal plasticity simulations of roping from experimental microstructures

Comparing the spacing of grain clusters in figure 3(*a*) with the spacing between the undulations observed on the surface of the sheet in figure 4, one sees a difference in scale of approximately an order of magnitude. In order to make a quantitative link between the microstructure and the surface roughness crystal plasticity, simulations must be performed. The VPFFT technique, described in detail below, has been used to quantitatively predict the surface roughness profile starting from the EBSD map shown in figure 3(*b*). Unlike previous crystal plasticity simulations described in the introduction, this work has focused on the through-thickness microstructure and the importance of considering the local environment on an embedded grain's ability to undergo out-of-plane shear. A second set of simulations have been performed using the VPSC code, in which the local environment of each pixelized crystal orientation is exactly the same, thus providing us with a reference case to assess the importance of using spatially resolved simulations to predict the overall roping behaviour. While there have been significant advances in the three-dimensional measurement of microstructure and microtexture via EBSD [16–18] the ability to measure volumes large enough to capture the wavelength of surface roughness
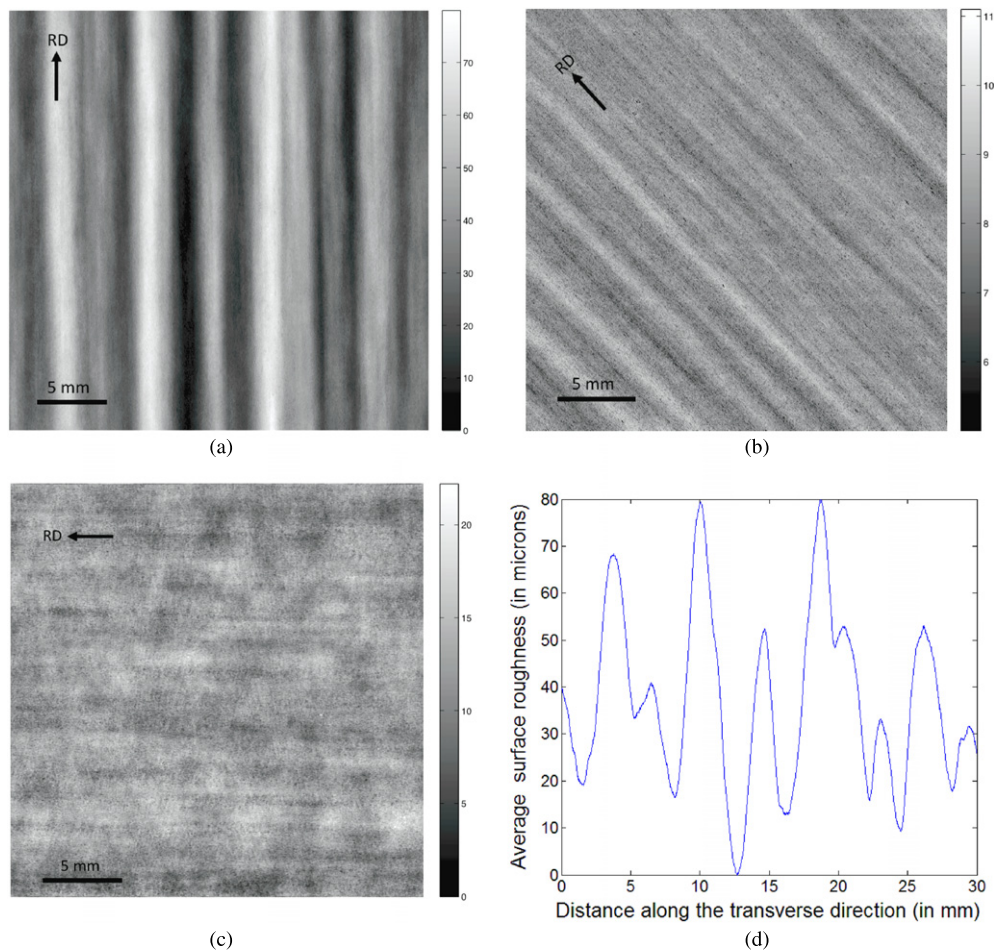
Figure 4. Profilometry measurements over 30 mm by 30 mm regions from the surface of samples tested in tension to 15% elongation parallel to the (*a*) prior RD (*b*) 45° to RD and (*c*) parallel to TD. In each case the tensile direction is vertical. The scale to the right of each figure gives the surface height in micrometres. The two-dimensional roughness map in (*a*) has been averaged parallel to RD to give the one-dimensional trace in (*d*).

observed in figure 4 and implement it in full-field crystal plasticity simulations is still limited. Therefore, here we focus on two-dimensional measurements of local orientations.

3.1. Full-field simulations using the VPFFT code

A detailed description of the VPFFT model has been given elsewhere [15, 19] and will not be reproduced here. The key concept in this approach is that Green's function method is used to solve the governing equations of equilibrium of stresses and compatibility of deformations for a periodic polycrystal. This method requires the computation of convolutions between Green's function associated with the velocity field G_{ij} and a polarization field φ_{ij}, suitably determined from the heterogeneity of the material (see [15, 19] for details). These convolutions become mere multiplications in Fourier space, allowing for a very efficient solution of the governing equations (in which the polarization is iteratively adjusted until equilibrium and compatibility

are fulfilled), and (particularly relevant to roping predictions) the *a posteriori* computation of the displacement field. This methodology leads to significant computational efficiency, compared with a finite element solution of the same problem, with the same resolution [20, 21].

In particular, the fluctuation (symbol '$\sim$') of the velocity field is given by the following convolution integral in Cartesian space:

$$\tilde{v}_k(\boldsymbol{x}) = \int_{R^3} G_{ki,j}(\boldsymbol{x} - \boldsymbol{x}')\varphi_{ij}(\boldsymbol{x}')\,\mathrm{d}\boldsymbol{x}' \tag{2}$$

which can be solved in Fourier space as

$$\hat{\tilde{v}}_k(\xi) = (-i\xi_j)\hat{G}_{ki}(\xi)\hat{\varphi}_{ij}(\xi), \tag{3}$$

where the symbol '$\hat{}$' indicates Fourier transform and ξ is a Fourier space's frequency. Antitransforming equation (3), the new position of each material point $\boldsymbol{x}$ that coincides with a Fourier point can be obtained as

$$x_i = X_i + (\dot{E}_{ij}X_j + \tilde{v}_i(\boldsymbol{x}))\Delta t, \tag{4}$$

where Δt is the time increment corresponding to one deformation step. A consequence of the above-described method is that the solution obtained is fully periodic. In our simulations we have started from the two-dimensional EBSD map shown in figure 3(*b*), such that a regular grid of $2^{11} \times 2^9$ (along TD and ND, respectively) = 1048 576 EBSD measurement points (each point having associated a crystallographic orientation) were used as Fourier points in the crystal plasticity simulation. Because of periodicity, this two-dimensional microstructure input should be considered as being extruded in the third dimension (parallel to the prior RD). While this is expected to accentuate the tendency for shearing and rigid body rotation about the RD, Sinclair [13] has shown that the effect is not dominant and that the effect quickly saturates with the length of the grains parallel to the RD direction.

Another aspect to be considered, arising from the unavoidable periodicity of the unit cell used for the present roping predictions, comes from the need of having traction-free surfaces at the top and bottom of the simulation domain. In order to accomplish this, the method outlined in [19] has been followed. The bottom five layers of Fourier points normal to ND were replaced by a second phase having infinite compliance (i.e. identically zero stress). In this way a 'buffer zone' is created that separates the top and bottom surfaces of the simulation domain when the periodic nature of the simulation box is considered.

Calculations were carried out using the VPFFT technique to simulate uniaxial tension by imposing a macroscopic tensile strain-rate component parallel to either the RD or TD directions, for comparison with the experiments in figures 4(*a*) and (*c*). In the direction transverse to the tensile direction (i.e. either the TD or RD directions, respectively) the macroscopic stresses were assumed to be zero. As noted above, the stresses in the ND are also zero due to the buffer layer. All macroscopic shear stresses were also assumed to be zero. Slip was considered to occur on the $\{1\,1\,0\}\langle1\,1\,1\rangle$ and $\{1\,1\,2\}\langle1\,1\,1\rangle$ slip systems. A constant critical resolved shear stress (CRSS) was assumed and crystallographic orientations were kept fixed (i.e. no microstructure evolution was considered). Simulations were performed in steps of 0.01 macroscopic average tensile strain to a maximum of 0.15 strain.

From these simulations, the incremental displacements of each Fourier point belonging to the top surface of the simulation cell have been calculated according to equation (4) for comparison against the experimentally measured surface profiles in figure 4. Moreover, the resulting strain field has been used to examine the spatial correlations of the deformation response. In particular, the shear strain component, ε_{12} (1 = TD, 2 = ND) associated with the out-of-plane shear envisioned in the Takechi has been evaluated.

3.2. Mean-field simulations using the VPSC code

To examine the significance of the full-field VPFFT simulations in terms of considering local interactions, and particularly the shearing tendency of grains, simulations of the deformation of individual grains have been performed with the VPSC code, utilizing the same dataset as used for the VPFFT simulations. Under the VPSC formulation each orientation is considered to be embedded in an effective homogeneous medium whose properties are those corresponding to the macroscopic average over the entire polycrystal. Following the same scheme as previously used by Engler *et al* [7], each crystal orientation associated with each pixel of our orientation image was considered to be embedded in a homogeneous matrix.

Also following [7], a very compliant matrix behaviour was assumed by setting the constitutive parameter n^{eff} to 100 (see [8] for details). In this way, the deformation of each individual orientation was almost independent of its neighbourhood, and was assessed particularly for its tendency for out-of-plane shearing. These results were subsequently mapped back onto the original EBSD map to compare against the VPFFT simulation results.

The same macroscopic boundary conditions, slip systems and CRSS as in the VPFFT simulations were used in these simulations, which were only performed for tension parallel to RD.

4. Comparison between experimental and simulated roping profiles as predicted by VPFFT

The net vertical displacement of the Fourier points along the top surface of the simulation cell (figure 3(*b*)) calculated with VPFFT are shown in figure 5, for simulations performed with the TA oriented parallel to RD and TD. Qualitatively, the simulations give the correct prediction with respect to the effect of orientation of the TA on the magnitude of the roping. While the simulation performed parallel to RD shows a large-scale undulation on a scale much larger than the size of an individual grain, the simulation performed with tension parallel to the TD direction shows only a relatively weak surface roughness with no large-scale features appearing.

The predicted low roughness amplitude for the test performed parallel to TD is a direct consequence of the extruded grain shape arising from the periodicity of the simulation cell in the third dimension. This configuration results in the long axis of the grains being oriented perpendicular to the TA when the test is performed parallel to TD. As has been pointed out previously [13], such a geometrical configuration strongly resists the shearing tendency of grains and therefore effectively suppresses roping.

The results of the simulation performed with the TA parallel to RD can be directly compared with the experimentally measured surface roughness shown in figure 4(*d*). Figure 6 shows the results from figure 4(*d*) and 5 plotted side by side. While the simulation domain is much smaller than the experimentally measured one, an excellent agreement is shown between both the wavelength and amplitude of the large-scale surface roughness predicted by the VPFFT simulations and experiments. As mentioned above, the R_q value measured experimentally from the two-dimensional map was 18 μm. While the simulation domain was only large enough to see roughly one wavelength, one sees that the predicted R_q value would be of the order of 15.5 μm, very similar to the experimental value.

One can further investigate the source of the surface profile for the simulation performed parallel to RD by examining the spatial distribution of the out-of-plane shear strain. Figure 7 shows the out-of-plane shear strain field after the first deformation increment of 1% (note that, since no microstructure evolution has been considered, this field is simply proportional to the
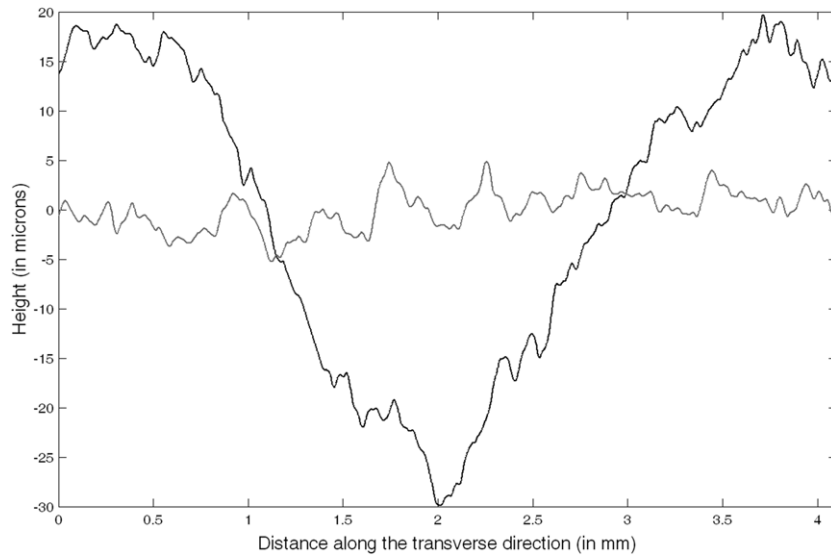
Figure 5. Effect of the tensile testing direction on the amplitude of surface roughness after 15% tensile strain. The black curve corresponds to a tension along the RD, and the grey curve corresponds to a tension along the TD. The response is qualitatively similar to the experimental data in figures 4(*a*) and (*c*).
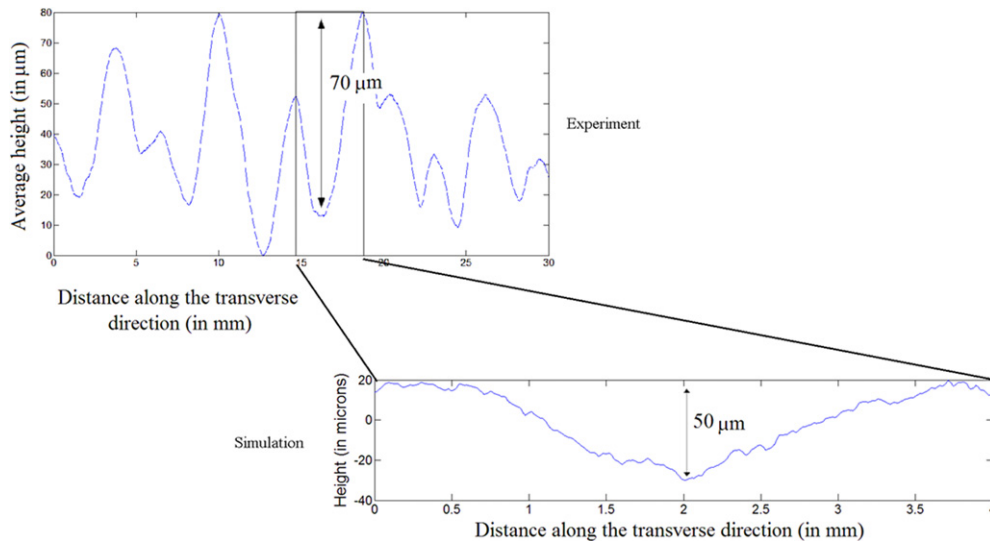

Figure 6. Comparison of surface roughness from experiment (figure 4(*d*)) and simulation, showing very good quantitative agreement for both the wavelength (about 4–5 mm along the TD) and the amplitude.

same shear strain field, evaluated at a different deformation level). In this figure one can see two predominant clusters of grains. Near the bottom left of the figure one can see a cluster of grains where the net tendency is for negative shearing (large proportion of dark grains). As can be seen, the size of this cluster corresponds very closely to the length of the surface
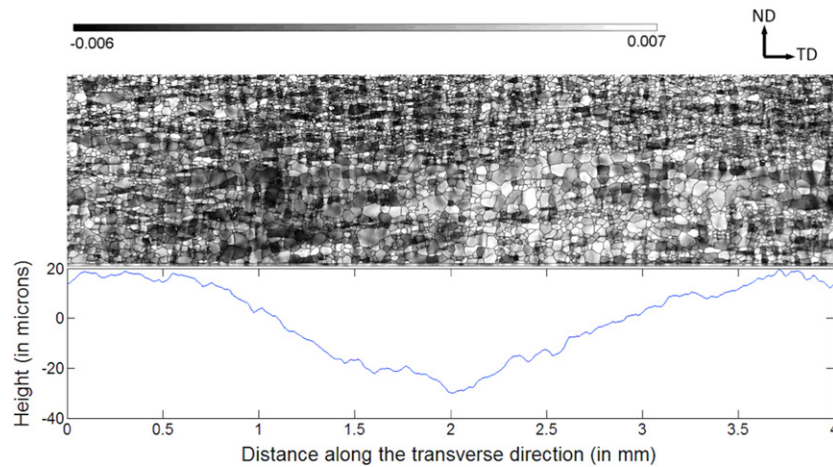
Figure 7. A map (top) of the spatial distribution of shear strain component ε_{12} after a VPFFT simulation of 1% elongation parallel to RD. The legend above the maps gives the correspondence between grey level and out-of-plane shear strain. Regions containing clusters of grains having a net positive (grey to white) and negative (grey to black) shearing tendency are observed, the former particularly on the right-hand side of the map, the latter on the left-hand side. Directly beneath the map, the predicted surface displacement profile (as shown in figure 6) is seen. The dark cluster of negatively shearing grains in the map corresponds to the negative slope of the surface on the left and the light cluster of positively shearing grains in the map corresponding to the positive surface displacement on the right.

profile with a negative slope. Similarly, on the right-hand side of the cell a cluster having a net positive shearing tendency (large proportion of light coloured grains) can also be observed. This also corresponds closely to the portion of the surface profile having a positive slope. It is important to note that the EBSD map in figure 3(b) alone gives no indication of these clusters.

5. Influence of the local neighbourhood on the shearing tendency of grains

As seen in figure 7, the tendency of individual grains within close proximity of one another to shear in a similar way leads to the long wavelength surface displacements that cause roping. It was shown in a previous paper [13] that the local environment of a grain can significantly influence its tendency to undergo out-of-plane shearing. For example, a grain that in isolation would tend to shear may not if it is embedded in a matrix whose shearing tendency is opposite. Alternatively, orientations that would tend to exhibit no tendency for rotation may themselves rotate if embedded in a matrix of grains that does wish to rotate.

In order to examine the importance of the local environment on the spatial distribution of strains, the VPFFT results presented above have been compared with mean-field simulations. Figure 8 shows histograms of the out-of-plane shear strains predicted by both simulations at 1% macroscopic strain along RD. The mean-field predictions show a large number of grains with a strong positive and negative shear tendency, as well as a large number of grains with little or no shear tendency (figure 8(a)). The full-field predictions, on the other hand, show fewer grains having a strong shearing tendency, and instead predict a larger fraction of grains having low shearing tendency (figure 8(b)). The net effect of the local neighbourhood, as captured by the VPFFT simulations, is therefore to moderate the shearing tendency of individual grains due to the constraints imposed by their surroundings.
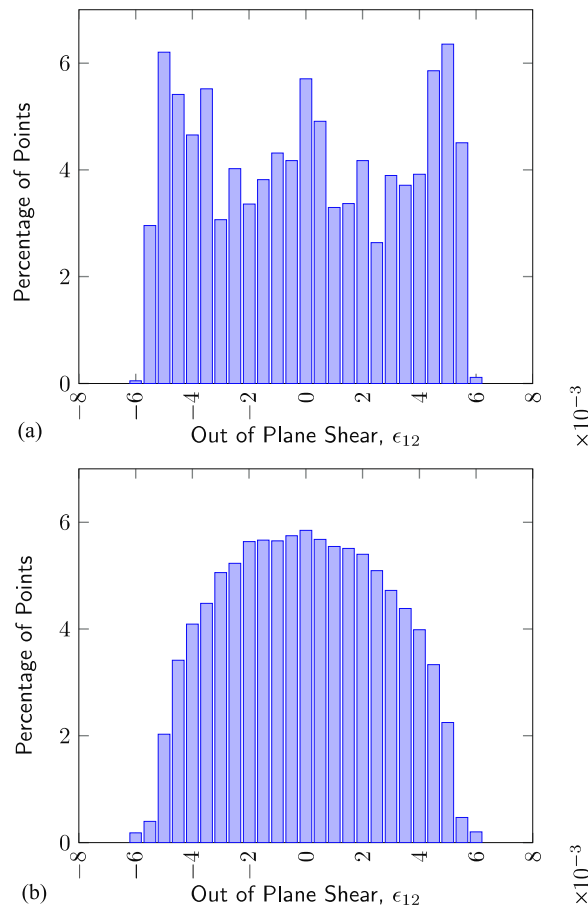
Figure 8. Out-of-plane shear strain distribution predicted by (*a*) mean-field and (*b*) full-field simulations after 1% tensile deformation parallel to the RD.

This can be examined further by mapping the shear strains onto the microstructure, as shown in figure 9. To simplify the interpretation, the shearing tendency has been separated into black regions exhibiting large positive shearing tendency ($0.007 > \varepsilon_{12} > 0.002$), white regions exhibiting large negative shearing tendency ($-0.006 < \varepsilon_{12} < -0.002$) and grey regions exhibiting low shearing tendency ($0.002 > \varepsilon_{12} > -0.002$). One can see similar features in the maps arising from the full-field and mean-field simulations, mainly large clusters of grains having high positive and negative shearing tendency, as already noted above. However, the maps do have significant differences. Importantly, the mean-field map shows many more cases of white and black regions being adjacent to one another, whereas the VPFFT simulations show many more low shearing (grey) regions and few regions where white and black areas are in direct contact.

This tendency for regions of high positive and negative shearing to not be adjacent to one another in the VPFFT simulations can be quantified by counting the number of black/white, black/grey and white/grey points that neighbour one another in figures 9(*a*) and (*b*). To do this, the four nearest neighbours to each point in figures 9(*a*) and (*b*) were analysed and counted, the results being shown in figure 10. One can see that the total number of black/grey and
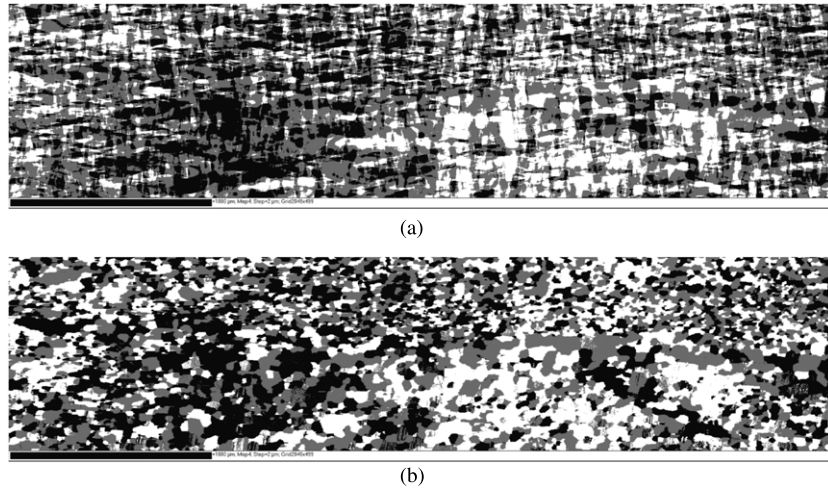
(a)

(b)

Figure 9. Distribution of out-of-plane shear strain intensity calculated with (*a*) the VPFFT model and (*b*) the VPSC model. The black regions exhibit large negative shear intensity ($-0.006 < \varepsilon_{12} < -0.002$), the grey regions exhibit medium shear intensity ($-0.002 < \varepsilon_{12} < 0.002$), and the white regions exhibit large positive shear intensity ($0.002 < \varepsilon_{12} < 0.007$).
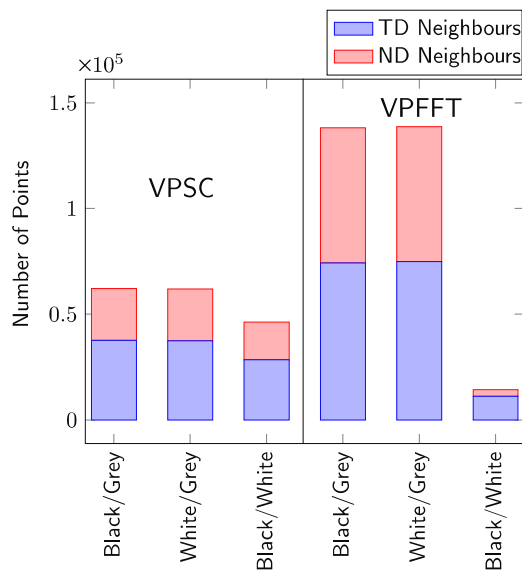

Figure 10. Each point comprising figures 9(*a*) and (*b*) was examined to deduce the shearing tendency (high negative = black, low = grey, high positive = white) of its four nearest neighbours. The neighbouring points having a different shearing tendency compared with the central point were identified and counted. The neighbours have been further identified based on whether they neighbour the central point parallel to TD (horizontal in figure 9) or parallel to ND (vertical in figure 9).

white/grey neighbours is larger in the full-field simulations compared with the mean-field results. This arises from the fact that the strains associated with the same orientation are identical under the mean-field approach, whereas the VPFFT simulations allow for variations of strain within individual grains. The second point that is immediately apparent is that

the number of black/white neighbouring points is significantly larger in the mean-field case compared with the VPFFT simulation. Thus, consistent with figure 8, these results indicate that the local neighbourhood of a point in the VPFFT simulation tends to suppress strong differences in shearing behaviour between neighbouring orientations. The tendency to suppress local differences in shearing tendency can also be seen to be anisotropic. In figure 10 the data are separated into points that neighbour one another parallel to the TD (horizontal direction in figure 9) and parallel to the ND (vertical direction in figure 9). In the mean-field simulation, of the total number of black/white neighbours 39% are aligned parallel to the ND. In the full-field simulation this number drops to 22%. This indicates that the VPFFT simulations predict a stronger suppression of neighbouring opposite shearing tendencies when the points are neighbouring one another parallel to the ND, compared with when they are neighbouring one another parallel to the TD. This is physically consistent with the fact that opposing shearing tendencies parallel to TD can be easily accommodated as envisioned originally by the Takechi model for roping (cf figure 1). The fact that neighbouring grains through the thickness direction of the sheet more strongly interact with one another is an important observation in terms of the phenomenon of roping. This observation is consistent with the work of Wilson *et al* [22, 23] and more recently Wu *et al* [24, 25], in which the surface roughening was found to depend not only on surface grains but also to the through-thickness distribution of grains and their deformation. This is also consistent with the observations of Wu *et al* [26] who found that interactions between grains in the ND plane were relatively weak. This was responsible for the good prediction of their SRM model (which does not explicitly account for neighbour interactions) compared with a full 2D FEM simulation performed in the same plane.

The suppression of opposing shearing tendency when points are neighbouring one another in the ND is significant as it suggests that observations of the orientations in the RD plane may be more significant to explain experimentally observed surface roping than measurements made in the ND plane. While a ND plane map may show significant banding of grains in a given plane, if similar banding of grains having the opposite tendency for shearing occurs above or below this plane then their individual effects will cancel leading to low levels of roping. Conversely, ND plane EBSD maps measured in a plane that does not cut through regions of significant orientation banding can lead to erroneous conclusions about a material's tendency for roping.

Finally, one can compare the mean-field and full-field results based on the correlation between orientation and shearing tendency. In order to examine this correlation, the orientation data from the EBSD map have been plotted as discrete data on the $\phi_2 = 45°$ section of the ODF and coloured based on the magnitude of the shear strain ε_{12}. Because the shearing shown in figure 1 does not obey orthorhombic sample symmetry, the ODFs are plotted using triclinic sample symmetry.

Figure 11 shows the results of this analysis plotted separately for the full-field (*b*), (*d*), (*f*) and mean-field (*a*), (*c*), (*e*) simulations. The latter results are essentially the same as those presented by Engler *et al* [7] and show that the orientations that exhibit strong shearing extend from the low index {1 1 1}⟨1 1 0⟩ type orientations envisioned in the Takechi model towards the high index orientations of the type {2 2 3}[5 8 2] experimentally observed here (cf figure 2). Comparing these results with those obtained from the VPFFT simulation illustrates again the strong effect the local neighbourhood has on perturbing the behaviour of individual orientations. Indeed, it can be found that orientations that are predicted to shear in the positive sense when embedded within a homogenous and rather compliant matrix can be forced to shear in a negative sense in the VPFFT simulation. This occurs at instances where the orientation is in a neighbourhood where the neighbours prefer to shear in the opposite sense. In contrast to the hypothesis made in [13], the main effect of the local neighbourhood seems not to cause
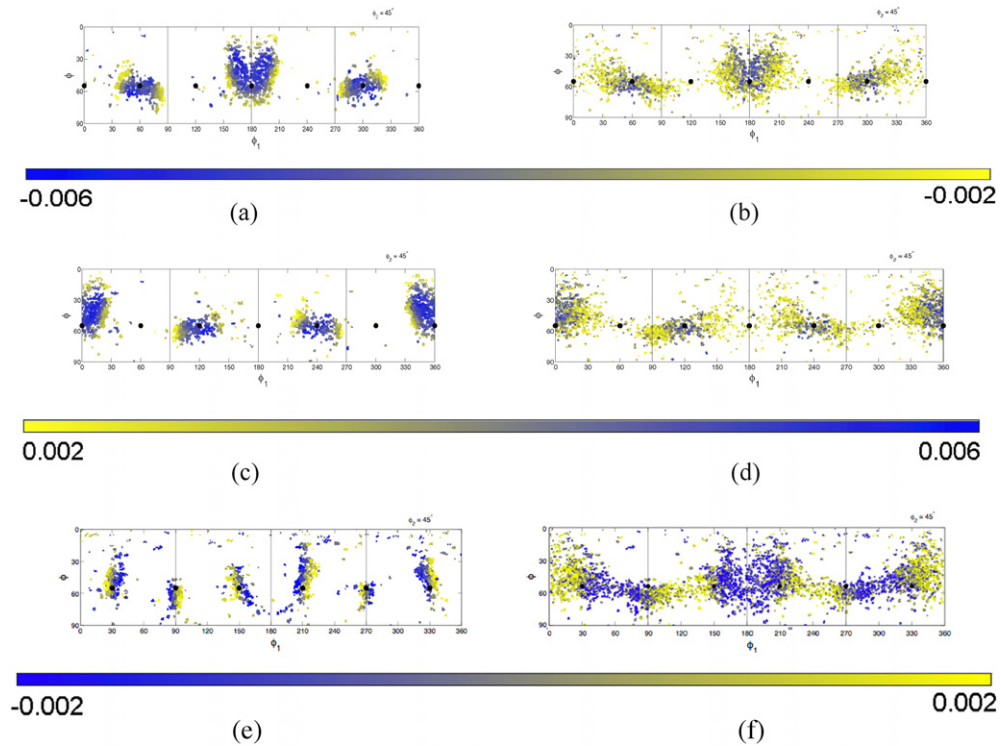
Figure 11. Simulation data plotted in $\phi_2 = 45°$ section of the ODF. Each point is coloured corresponding to the predicted out-of-plane shear strain (ε_{12}) as indicated by the corresponding scales bars. The data have been separated into orientations exhibiting large positive shear (*a*), (*b*), low shear (*c*), (*d*) and large negative shear (*e*), (*f*). The data are separated according to simulation type. Plots (*a*), (*c*) and (*e*) are from VPSC simulations while (*b*), (*d*) and (*e*) are from VPFFT simulations.

orientations having a low tendency for shearing (when considered in isolation) to shear because of neighbouring strongly shearing grains, but instead to strongly perturb the shearing behaviour of the orientations expected to exhibit the largest shearing tendency.

6. Conclusion

In this paper, we have presented both experiments and simulations of roping of a ferritic stainless steel. It has been shown that the full-field VPFFT simulations performed on an experimentally measured microstructure can predict both the amplitude and wavelength of roping when the experimental data used are taken from the RD plane rather than the more commonly investigated ND plane. It has been shown that the neighbour–neighbour interactions tend to strongly perturb the behaviour of orientations that tend to cause shearing. Notably, it is observed that the influence of neighbouring strongly positive and strongly negative shearing orientations on one another is stronger when the neighbours are oriented through thickness. This corresponds to a cancelling out of the shearing tendency of the two opposite behaviours and leads to an attenuation of the surface roughening. Such an effect cannot be captured from microstructural observations in the ND plane alone. Such observations help us to better understand the complex and long empirically known inter-relationships between roping, microstructure and processing.

15

Acknowledgments

References

[1] Chao H C 1967 *Trans. Am. Soc. Met.* **60** 37
[2] Takechi H, Kato H, Sunami T and Nakayama T 1967 *Trans. JIM* **8** 233
[3] Wright R N 1972 *Metall. Trans.* **3** 83
[4] Baczynski J, Guzzo R, Ball D and Lloyd D J 2000 *Acta Mater.* **48** 3361
[5] Sheppard T and Richards P 1986 *Mater. Sci. Technol.* **2** 693
[6] Sztwiertnia K, Pospiech J and Rostek T 1999 *Proc. 12th Int. Conf. on Textures of Materials* 647
[7] Engler O, Huh M Y and Tomé C N 2005 *Metall. Mater. Trans.* A **36** 3127
[8] Lebensohn R A and Tomé C N 1993 *Acta Metall. Mater.* **41** 2611
[9] Tomé C N and Lebensohn R A 2011 VPSC Version7c, Los Alamos National Laboratory, USA
[10] Shin H J, Am J K, Park S H and Lee D N 2003 *Acta Mater.* **51** 4693
[11] Wu P D, Lloyd D J, Bosland A, Jin H and Macewen S R 2003 *Acta Mater.* **51** 1945
[12] Wu P D, Jin H, Shi Y and Lloyd D L 2006 *Mater. Sci. Eng.* A **423** 300
[13] Sinclair C W 2007 *Metall. Mater. Trans.* A **38** 2435
[14] Moulinec H and Suquet P 1998 *Comput. Methods Appl. Mech. Eng.* **157** 69
[15] Lebensohn R A 2001 *Acta Mater.* **49** 2723
[16] Rowenhorst D J, Gupta A, Feng C R and Spanos G 2006 *Scr. Mater.* **55** 11
[17] Zaefferer S, Wright S I and Raabe D 2008 *Metall. Mater. Trans.* A **39** 374
[18] Jin H, Wu P D, Ball M D and Lloyd D J 2005 *Mater. Sci. Technol.* **21** 419
[19] Lebensohn R A, Brenner R, Castelnau O and Rollett A D 2008 *Acta Mater.* **56** 3914
[20] Prakash A and Lebensohn R A 2009 *Modelling Simul. Mater. Sci. Eng.* **17** 064010
[21] Liu B, Raabe D, Roters F, Eisenlohr P and Lebensohn R A 2010 *Modelling Simul. Mater. Sci. Eng.* **18** 085005
[22] Wilson D V, Roberts W T and Rodrigues P M B 1981 *Metall. Trans.* A **12** 1595
[23] Wilson D V, Roberts W T and Rodrigues P M B 1981 *Metall. Trans.* A **12** 1603
[24] Wu P D and Lloyd D J 2004 *Acta Mater.* **52** 1785
[25] Wu P D, Lloyd D J, Jain M, Neale K W and Huang Y 2007 *Int. J. Plasticity* **23** 1084
[26] Wu P D, Lloyd D J and Huang Y 2006 *Mater. Sci. Eng.* A **427** 241